

This is a repository copy of *Genomic signatures of vegetable and oilseed allopolyploid Brassica juncea and genetic loci controlling the accumulation of glucosinolates*.

White Rose Research Online URL for this paper:
<https://eprints.whiterose.ac.uk/178702/>

Version: Accepted Version

Article:

Bancroft, Ian orcid.org/0000-0001-7707-1171 and He, Zhesi orcid.org/0000-0001-8335-9876 (Accepted: 2021) Genomic signatures of vegetable and oilseed allopolyploid Brassica juncea and genetic loci controlling the accumulation of glucosinolates. Plant biotechnology journal. ISSN 1467-7644 (In Press)

<https://doi.org/10.1111/pbi.13687>















Reuse

Items deposited in White Rose Research Online are protected by copyright, with all rights reserved unless indicated otherwise. They may be downloaded and/or printed for private study, or other acts as permitted by national copyright laws. The publisher or other rights holders may allow further reproduction and re-use of the full text version. This is indicated by the licence information on the White Rose Research Online record for the item.

Takedown

If you consider content in White Rose Research Online to be in breach of UK law, please notify us by emailing eprints@whiterose.ac.uk including the URL of the record and the reason for the withdrawal request.

Modelling of gene loss propensity in the pangenomes of three *Brassica* species suggests different mechanisms between polyploids and diploids

Philipp E. Bayer¹ , Armin Scheben¹, Agnieszka A. Golicz², Yuxuan Yuan¹ , Sebastien Faure³, HueyTyng Lee⁴ , Harmeet Singh Chawla⁴, Robyn Anderson¹, Ian Bancroft⁵ , Harsh Raman⁶ , Yong Pyo Lim⁷, Steven Robbins⁸, Lixi Jiang⁹ , Shengyi Liu¹⁰ , Michael S. Barker¹¹, M. Eric Schranz¹² , Xiaowu Wang¹³ , Graham J. King¹⁴ , J. Chris Pires¹⁵ , Boulos Chalhoub⁹, Rod J. Snowdon⁴ , Jacqueline Batley¹  and David Edwards^{1,*} 

¹School of Biological Sciences and the Institute of Agriculture, Faculty of Science, The University of Western Australia, Crawley, WA, Australia

²Plant Molecular Biology and Biotechnology Laboratory, Faculty of Veterinary and Agricultural Sciences, University of Melbourne, Parkville, VIC, Australia

³Innolea SAS, Mondonville, France

⁴Department of Plant Breeding, IFZ Research Centre for Biosystems, Land Use and Nutrition, Justus Liebig University Giessen, Giessen, Germany

⁵Department of Biology, University of York, York, UK

⁶NSW Department of Primary Industries, Wagga Wagga Agricultural Institute, PMB, Wagga Wagga, NSW, Australia

⁷Department of Horticulture, Chungnam National University, Daejeon, South Korea

⁸BASF Innovation Center, Gent, Belgium

⁹Institute of crop science, Department of Agronomy and Plant Breeding, Zhejiang University, Hangzhou, China

¹⁰Chinese Academy of Agricultural Sciences, Oil Crops Research Institute, Wuhan, China

¹¹Department of Ecology & Evolutionary Biology, University of Arizona, Tucson, AZ, USA

¹²Biosystematics Group, Wageningen University and Research Center, Wageningen, The Netherlands

¹³Institute of Vegetables and Flowers, Chinese Academy of Agricultural Sciences (IVF, CAAS), Beijing, China

¹⁴Southern Cross Plant Science, Southern Cross University, Lismore, NSW, Australia

¹⁵Division of Biological Sciences, Bond Life Sciences Center, University of Missouri, Columbia, Missouri, USA

Received 28 January 2021;

revised 11 July 2021;

accepted 20 July 2021.

*Correspondence (Tel +61 (08) 6488 2415;

fax +61 (08) 6488 1108; email

dave.edwards@uwa.edu.au)

Keywords: *Brassica*, pangenome,

XGBoost, gene loss propensity,

machine learning, transposable

elements.

Summary

Plant genomes demonstrate significant presence/absence variation (PAV) within a species; however, the factors that lead to this variation have not been studied systematically in *Brassica* across diploids and polyploids. Here, we developed pangenomes of polyploid *Brassica napus* and its two diploid progenitor genomes *B. rapa* and *B. oleracea* to infer how PAV may differ between diploids and polyploids. Modelling of gene loss suggests that loss propensity is primarily associated with transposable elements in the diploids while in *B. napus*, gene loss propensity is associated with homoeologous recombination. We use these results to gain insights into the different causes of gene loss, both in diploids and following polyploidization, and pave the way for the application of machine learning methods to understanding the underlying biological and physical causes of gene presence/absence.

Introduction

A single reference genome does not represent the gene content of a species due to gene presence/absence variation (PAV) between individuals. In plants, genome duplication through polyploidization provides an opportunity for differential gene loss and subsequent presence/absence variation between individuals, and species that have experienced relatively recent polyploidy often host a relatively high proportion of dispensable genes. Several studies have examined gene conservation and loss following polyploidization. Neofunctionalization of duplicated genes has been observed in cotton (Adams *et al.*, 2003; Rong

et al., 2010; Yang *et al.*, 2017), while in *Brassica napus*, homoeologous exchange (HE) between chromosomes is associated with gene loss (Hurgobin *et al.*, 2018) and with the generation of novel chimeric genes (Zhang *et al.*, 2020).

Differential fractionation of genomes has been observed following ancient triplication in the diploid *Brassica* species *B. rapa* and *B. oleracea* (Cheng *et al.*, 2014), while in octoploid strawberry (*Fragaria ananassa*), the diploid *F. vesca* subgenome dominates the other three subgenomes, having lost the fewest genes (Edger *et al.*, 2019). Differential loss and retention of genes following two rounds of polyploidy has been reported in hexaploid bread wheat (*Triticum aestivum*) (Berkman *et al.*,

Please cite this article as: Bayer, P. E., Scheben, A., Golicz, A. A., Yuan, Y., Faure, S., Lee, H., Chawla, H. S., Anderson, R., Bancroft, I., Raman, H., Lim, Y. P., Robbins, S., Lixi Jiang, Liu, S., Barker, M. S., Schranz, M. E., Wang, X., King, G. J., Pires, J. C., Chalhoub, B., Snowdon, R. J., Batley, J. and Edwards, D. (2021) Modelling of gene loss propensity in the pangenomes of three *Brassica* species suggests different mechanisms between polyploids and diploids. *Plant Biotechnol. J.*, <https://doi.org/10.1111/pbi.13674>

2013), and differential subgenome retention and loss of genes has similarly been observed following tetraploidy in maize (Schnable *et al.*, 2011; Woodhouse *et al.*, 2010).

Amphidiploid *B. napus* (AC subgenome, $2n = 36$) formed approximately 7500 years ago following hybridization of *B. oleracea* (C genome, $2n = 18$) and *B. rapa* (A genome, $2n = 20$) (Allender and King, 2010; Nagaharu, 1935). It is believed that the A subgenome is derived from an ancestor of European turnip, while the C subgenome derives from a common ancestor of kohlrabi, cauliflower, broccoli and Chinese kale (Lu *et al.*, 2019), with the polyploid forming post domestication, with no apparent wild forms of *B. napus*. There is little support for a polyphyletic origin for *B. napus*, though there is evidence of introgression from *B. rapa/B. oleracea* after polyploidy (Allainguillaume *et al.*, 2006; An *et al.*, 2019). While there have been several studies of gene loss following polyploidy, these have either focused on individual plants which may not reflect species-level changes due to extensive gene presence/absence variation between individuals of the same species (Edger *et al.*, 2019; Edger *et al.*, 2017; Rong *et al.*, 2010; Yang *et al.*, 2017), or they have focused on resynthesized amphidiploids (Bird *et al.*, 2019). The datasets produced in pangenome studies offer a chance to investigate the physical mechanisms of gene loss using statistical approaches including machine learning.

In this study, we first produced a new genome assembly of *Brassica napus* cv. Darmor-*bzh*. Then we examined gene conservation and loss at the species level by constructing and comparing pangenomes for *B. napus* and its diploid progenitors *B. oleracea* and *B. rapa*. Comparative modelling of the propensity for gene loss in the three species revealed that in the diploids, genes with propensity for loss are primarily associated with transposable elements, while in the polyploid *B. napus*, propensity for gene loss was associated with the position of the gene on the pseudomolecule. By constructing pangenomes and applying a novel modelling method, this study presents the first assessment and comparison of the mechanisms that underlie gene presence/absence variation in a polyploid and its diploid progenitors.

Results and discussion

A new Darmor-*bzh* reference genome

A new 1192 Mbp Darmor-*bzh* reference genome was assembled, which is 342 Mbp (40%) larger than the previous v4 assembly (850 Mbp) (Chalhoub *et al.*, 2014), encoding 102 845 genes. The number of genes is similar to the 101 040 genes in the Darmor-*bzh* v4 annotation (Chalhoub *et al.*, 2014) and 94 586 to 100 919 genes in eight high-quality *B. napus* genomes (Song *et al.*, 2020). Both Darmor-*bzh* assemblies contain the same number of complete BUSCOs (423, 99.5%). The v9 assembly contains 14 duplicated BUSCOs that collapse into single copies in the v4 assembly (Table S1). Both assemblies are collinear (Figure S1a). In the new v9 assembly, pseudomolecules are larger by an average of 15.1 Mbp ranging from 3.8 Mbp (A03) to 59.5 Mbp (C02). The size of chromosome C02 is 105.7 Mb in the v9 assembly compared with 46.2 Mbp in the old assembly (Figure S1b). The new region on C02 is not due to misplacement as it does not align with any other region in the 4.1 assembly (Figure S1c). The majority of the additional sequence in the v9 assembly consists of repetitive and transposable elements, with the assembly repeat content increasing twofold from 319 Mbp in v4 (49%) to 643 Mbp in the v9 assembly (68%) (Table 1, Table S2, Figure S2). The percentage of repeats is higher than

reported in Song *et al.*, (2020), which may be due to different de novo repeat-finding pipelines. In the v9 assembly, the total size of all common repeat classes increased two-fold. For example, Helitron repeat content grew from 153 to 240 Mbp (Tables S2–S4). The difference in the size of C02 is explained by the difference in assembled repetitive elements: in v4.1, C02 contains 26 Mbp of repetitive elements, while in the v9 assembly, C02 contains 91 Mbp of repeats.

Construction of three new pangenomes

Using the iterative mapping and assembly approach (Bayer *et al.*, 2020; Hurgobin and Edwards, 2017), we have assembled pangenomes for *B. oleracea*, *B. rapa* and *B. napus*, representing the C, A and amphidiploid AC subgenomes, using 87, 77 and 79 individuals respectively (Table 2). Compared to the reference assemblies, each pangenome increased in size and gene content. The model of gene numbers converges asymptotically with the addition of each new individual suggesting that we have assembled almost all of the genes for these three species (Figure 1).

Annotation of the pangenomes predicted 58 315 gene-models in *B. oleracea*, 59 864 gene-models in *B. rapa* and 108 580 gene-models in *B. napus*. Out of these, 5963, 13 244 and 5735 gene-models are located on newly assembled pangenome contigs of the three pangenomes. Modelling of the pangenome size resulted in predicted total gene numbers for *B. oleracea*, *B. rapa* and *B. napus* of 58 347 (+/–2), 59 923 (+/–4) and 108 586 (+/–4), with predicted core gene numbers of 46 261 (+/–7), 40 391 (+/–11) and 65 096 (+/–150) respectively. The predicted pangenome size of *B. oleracea* is lower than the first *B. oleracea* pangenome which predicted a pangenome size of 63 865 +/31 (Golicz *et al.*, 2016) perhaps because the first pangenome used a wild relative in the calculations (*B. macrocarpa*), leading to a higher estimate in the first pangenome, but also used different annotation methods and repeat-masking methods. Similarly, the first *B. napus* pangenome predicted a pangenome size of 95 730 +/–11 (Hurgobin *et al.*, 2018), lower than what we observe here. When we exclude synthetic lines, the predicted *B. napus* gene number drops to 108 537 (+/–9), while the core gene number increases to 79 663 (+/–119). Therefore, while the addition of the synthetic lines only increases the predicted total gene number by 49 genes, the proportion of genes that demonstrate presence/absence variation increases from 26 to 38% (Table 3).

Our findings suggest that the synthetics contribute a greater diversity of gene combinations without significantly increasing gene number. The discrepancy in gene content between synthetic and non-synthetic *B. napus* lines is expected due to differential gene loss between the multiple independent polyploidization events. Natural *B. napus* is predicted to have derived from a single polyploidy event, while each of the 20 synthetic lines is more recently derived from combinations of 11 female and 14 male parents (Schmutzer *et al.*, 2015). Synthetic lines also demonstrate a greater diversity of homoeologous exchange events followed by subgenome-specific gene loss (Hurgobin *et al.*, 2018).

Brassica rapa and *B. oleracea* diverged from a common ancestor around 3 MYA (Sun *et al.*, 2019), so they may be expected to share a similar pangenome content. Based on read-alignments out of 58 315 *B. oleracea* genes, 57 729 (99%) are present in at least one *B. rapa* individual, and similarly, out of 59 864 *B. rapa* genes, 57 957 (97%) are present in at least one

Table 1 Assembly statistics for the newly assembled *B. napus* cv. Darmor-bzh v9 compared with v4.1 (Chalhoub *et al.*, 2014)

Assembly	Assembly size (Mb)	Anchored chromosome (Mb)	TEs (%)	Number of annotated genes	Completeness (BUSCO)
V4.1 (Chalhoub <i>et al.</i> , 2014)	850.3	645.4	46.5	101 040	99.5%
v9	1043.4	933.3	64.5	108 580	99.5%

Table 2 Pangenome additional contigs assembly statistics

Pangenome	Assembly size (Mbp)	Assembly N50	Predicted genes
<i>Brassica oleracea</i>	121.8	3848	6715
<i>Brassica rapa</i>	180.5	2500	19 767
<i>Brassica napus</i>	87.2	2295	5060

B. oleracea individual. Of the 108 580 *B. napus* genes, 105 149 (97%) and 106 977 (99%) are present in at least one individual of *B. oleracea* and *B. rapa* respectively (Figure 2, Table 3). *B. rapa* has a greater proportion of dispensable genes (33%) than *B. oleracea* (21%) (Figure S3), suggesting greater genetic diversity in *B. rapa*, which is in line with a higher genetic diversity observed in the A subgenome of *B. napus* (Wu *et al.*, 2019). Only 360, 711 and 955 genes were found to be unique in *B. oleracea*, *B. rapa* and *B. napus* respectively. Some of these are likely to be annotation artefacts or genes that have not yet been sampled in the other species, though this result does suggest that there may be genes unique to these species that could be of agronomic interest (Figure 3).

Gene loss specific to *B. Rapa* rapid cycling lines

PCA-clustering of *B. rapa* individuals identified a highly diverged cluster consisting of rapid cycling, self-compatible lines that have undergone intensive selection (FastPlants sc, FPSc). In these individuals, an additional 177 genes were found to be dispensable compared to the non-FPSc *B. rapa* individuals. Proteins encoded by these 177 genes share sequence identity with stress-response genes including HVA22 (a stress-response gene which regulates vesicular traffic (Brands and Ho, 2002)) and G-type lectin S-receptor-like serine/threonine-protein kinase SRK, a salinity-stress linked regulator (Sun *et al.*, 2013) which is also involved in self-incompatibility (Zhang *et al.*, 2011). The loss of these abiotic stress-related genes may be associated with faster growth of these plants. As the FPSc lines are self-compatible it may be expected that these lines have lost the self-incompatibility-linked genes *SLG*, *SRK* and *SCR/SP11* within the *S*-locus (Nasrallah, 1997). However, versions of these three genes are present in all of the FPSc lines, suggesting that self-compatibility in these lines is not caused by gene loss but rather by previously described polymorphisms (Kitashiba and Nasrallah, 2014).

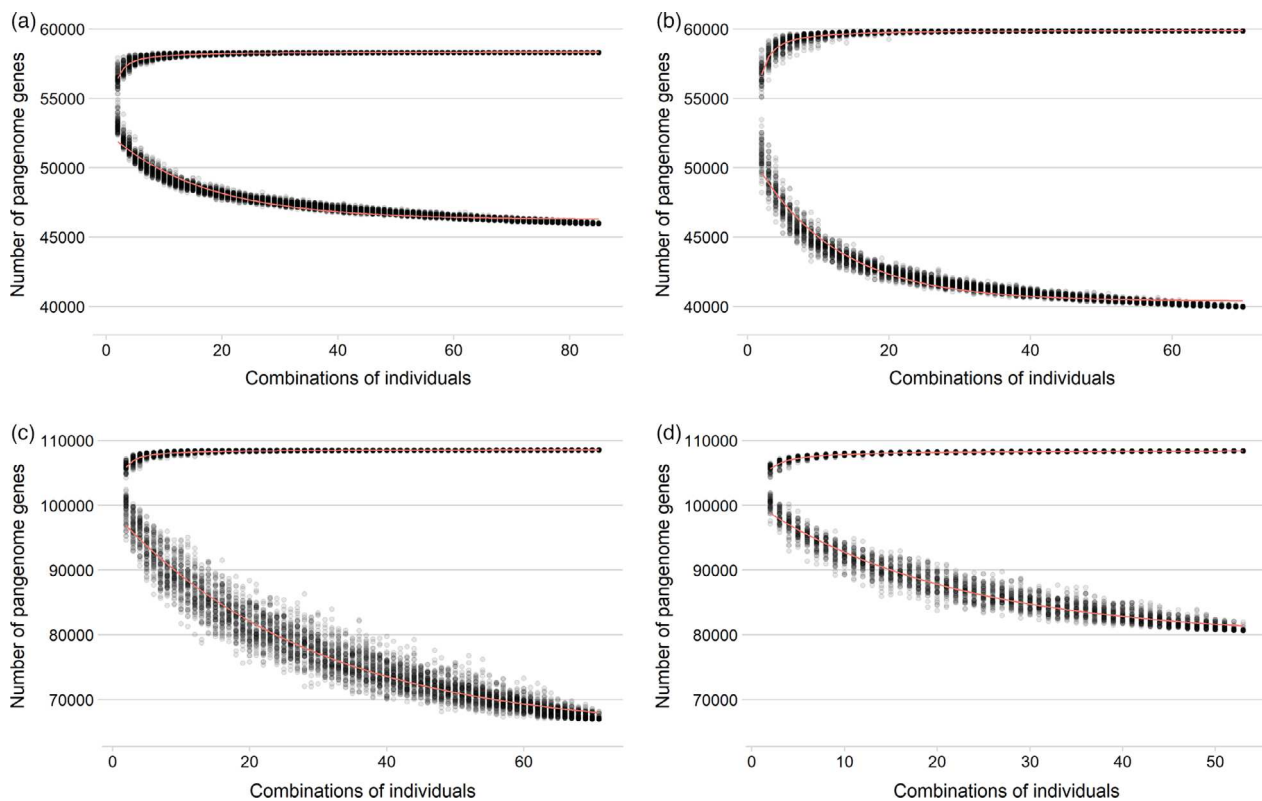
**Figure 1** Pangenome models based on the (Golicz *et al.*, 2016) gene number modelling method for (a) *B. oleracea*, (b) *B. rapa*, (c) *B. napus* (including synthetic lines) and (d) *B. napus* (excluding synthetic lines). Upper curves show the total pangenome after different combinations of individuals, the lower curve shows the number of core genes between all combinations of individuals.

Table 3 Shared genes between the three pangenomes based on exon-level read alignments. For *B. rapa*, FPSc (Fast Plants, self-compatible) and non-FPSc lines are compared. For *B. napus*, non-synthetic and synthetic lines are compared

	<i>B. oleracea</i> pangenome	<i>B. rapa</i> pangenome	<i>B. napus</i> pangenome
Total genes	58 315	59 864	108 580
Dispensable genes within the same species	12 354 (21%)	With FPScs 19 912 (33%) Without FPScs 19 735 (33%)	With synthetics 41 614 (38%) Without synthetics 27 930 (26%)
Core genes within the same species	45 961 (79%)	With FPScs 39 952 (67%) Without FPScs 40 129 (67%)	With synthetics 66 966 (62%) Without synthetics 80 650 (74%)
Present in all three species in at least one individual each	57 717 (99%)	57 941 (97%)	104 465 (96%)
Present only in...			
<i>B. napus</i> and <i>B. oleracea</i>	226 (0.4%)	0	648 (0.6%)
<i>B. napus</i> and <i>B. rapa</i>	0	1198 (2%)	2512 (2.3%)
<i>B. oleracea</i> and <i>B. rapa</i>	12 (0.02%)	16 (0.02%)	0
<i>B. napus</i>	0	0	955 (0.9%)
<i>B. rapa</i>	0	711 (1.1%)	0
<i>B. oleracea</i>	360 (0.6%)	0	0

Dispensable genes are commonly associated with abiotic and biotic stress

Dispensable genes are annotated predominantly with GO-terms associated with biotic and abiotic stress response for each of the three *Brassica* pangenomes (Table S5), with the term 'defense response' (GO:0006952) appearing significantly enriched in variable genes of *B. oleracea*, *B. rapa* and *B. napus*. Dispensability of stress response genes has been observed previously in crop pangenomes (Bayer *et al.*, 2019; Golicz *et al.*, 2016). In the *B. oleracea* pangenome, the GO terms 'response to salt stress' and 'defense to bacterium' were enriched in dispensable genes (Golicz *et al.*, 2016), while in the wheat pangenome, 'defense response' was among the GO terms with the greatest enrichment in dispensable genes (Montenegro *et al.*, 2017). Similar patterns were observed in the pangenomes of rice (Zhao *et al.*, 2018), *B. napus* (Hurgobin *et al.*, 2018), sesame (Yu *et al.*, 2019), pigeon pea (Zhao *et al.*, 2020), sunflower (Hübner *et al.*, 2019) and soybean (Liu *et al.*, 2020b), where biotic and abiotic stress resistance-related genes were enriched among variable genes.

The strong but variable selection pressure on disease resistance genes associated with the presence or absence of associated pathogens likely impacts their differential conservation and loss between individuals. We found 206, 379 and 445 nucleotide-binding leucine-rich repeat (NLR) genes in *B. oleracea*, *B. rapa* and *B. napus* respectively. The *B. oleracea* pangenome contained 89 fewer NLR genes than the *B. napus* C subgenome, while in contrast, the *B. rapa* A subgenome assembly contained 52 more NLR genes than the *B. napus* A subgenome. Many of these additional *B. rapa* NLR genes were not found in the *B. napus* reference assembly, highlighting the importance of pangenomes for species comparisons (Figure S4a). This pattern of differential loss was not apparent for two other classes of genes involved in disease resistance, RLP and RLK (Figure S4b), suggesting that the observed differences are not assembly artefacts and that there is a range of *R*-genes that are only present in the *B. rapa* gene pool and not in the *B. napus* gene pool.

Protein-protein interaction networks and the pangenome

Gene conservation and loss are associated with many factors. It has previously been observed that genes associated with protein-

protein interaction networks tend to be more resistant to loss following polyploidy than genes outside of such networks. However, this resistance to loss is also affected by selection, with a greater loss of networked genes in new polyploids under strong selection than those under more relaxed selection (Schoenrock *et al.*, 2017). This is exemplified in bread wheat, where the formation of the tetraploid occurred before domestication, while the hexaploid formed post domestication, with greater selection pressure that resulted in a greater loss of networked genes (Berkman *et al.*, 2013).

In our newly assembled *B. napus* pangenome, excluding synthetic lines, 86% of core genes are predicted to be in networks, while only 72% of dispensable genes are predicted to be in networks (Table S6). There was a statistically significant difference in network retention between the two subgenomes, with 91% and 81% of core genes within networks in the A and the C subgenomes, respectively (X^2 -test, $P < 0.005$ in all cases).

The retention of networked genes is slightly higher in the diploid species, with 87% and 90% of *B. oleracea* and *B. rapa* core genes predicted to be in networks compared with 86% of *B. napus* core genes in networks (Table S6), while only 68% and 70% of dispensable genes are predicted to be in networks. In the two diploids, as in *B. napus*, there was a statistically significant association between membership in protein interaction networks and variable genes (X^2 -test, $P < 0.005$). The diploid genomes may be under greater pressure to maintain networked genes, as the presence of a duplicate gene set in the polyploid may partially compensate for the loss of genes in functional networks.

Searching for A and C genome ancestors

Several genomic studies have attempted to identify the diploid parents of *B. napus* (Lu *et al.*, 2019; Song *et al.*, 2020). Here, we compared PAV patterns based on PCA between the two *B. napus* subgenomes and the *B. rapa* and *B. oleracea* individuals. This identified close relatives for the A subgenome (Figure 5a) but not for the C subgenome (Figure 5b), similar to previous observations based on SNPs, suggesting a complex origin for the C subgenome (Song and Osborn, 1992). We hypothesized that there may be different ancestors for different C subgenome chromosomes. We therefore repeated this analysis for each chromosome and observed inconsistencies between chromosomes (Figures S6 and S7). For example, A05 shows very little divergence between

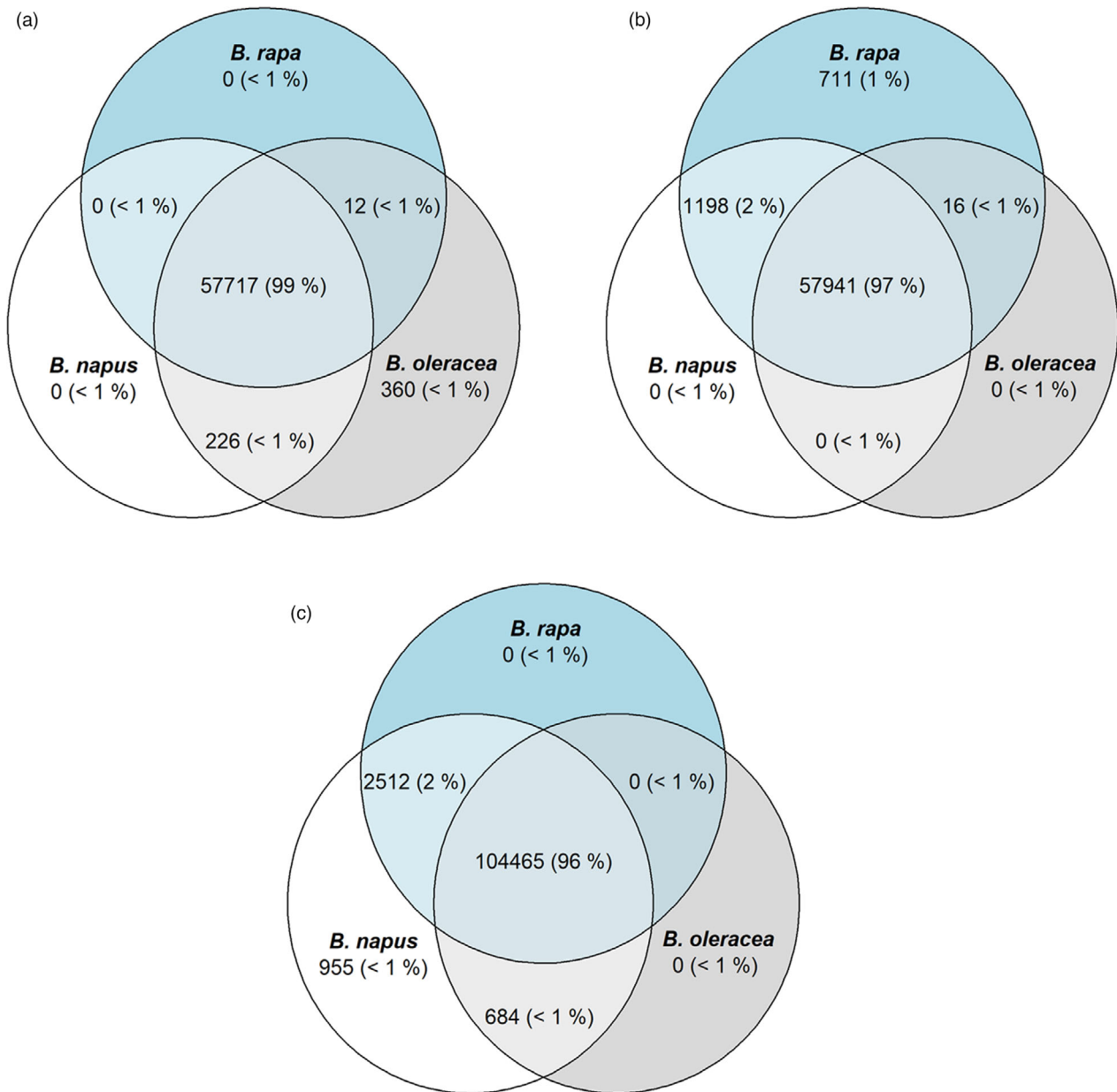


Figure 2 Genes shared across *B. oleracea*, *B. rapa* and *B. napus* in the three assembled pangenomes. (a) *B. oleracea* pangenome (58 315 genes), (b) *B. rapa* pangenome (59 864 genes) and (c) *B. napus* pangenome (108 580 genes).

individuals, which may be due to a previously described low frequency of homoeologous recombination of this chromosome (Pele *et al.*, 2017). C03 and C09 diverged the most, possibly due to elevated crossover frequency. However, we found no chromosome-specific ancestors, suggesting that the C-genome ancestors are not represented by the publicly available *B. oleracea* data.

Comparing transposon content between *B. oleracea*, *B. rapa* and *B. napus*

Many traits of agronomic interest in *B. napus* and its diploid ancestors have been linked with transposon insertions, including an LTR-insertion linked with resistance to pod shattering and silique length (Liu *et al.*, 2020a), and hAT, MITE and LINE

insertions linked with flowering time (Song *et al.*, 2020). In *B. napus*, a Helitron insertion within the promoter region of the self-incompatibility gene *BnSP11-1* has been linked with self-fertilization (Gao *et al.*, 2016). This insertion has not been observed in the diploid ancestors, suggesting that it arose after the formation of the polyploid *B. napus*.

Here most classes of transposons show a similar abundance between the A and C subgenomes of *B. napus* and their respective diploid ancestors *B. rapa* and *B. oleracea* (Tables S2–S4, S7–S12). For example, the percentage of hAT (DNA/DTA) elements ranged from 0.8 to 0.9% in *B. oleracea* and 0.5 to 0.8% in the C subgenome of *B. napus*, and a range of 0.7% to 0.9% in *B. rapa* compared with 0.6% to 0.9% in the A subgenome of *B. napus*. However, other classes of transposons

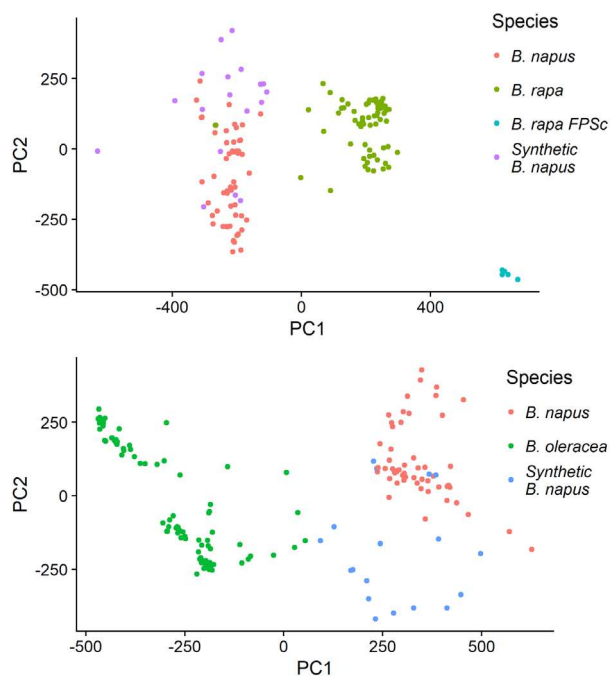


Figure 3 First two principal components based on PAV data of (a) A genome genes and (b) C genome genes. The PAV matrix of all *B. napus* genes was split into two subsets – (a) one containing only A-genome genes and A-genome species (*B. rapa*, fast-cycling *B. rapa* FPSc, *B. napus*) and (b) one containing only C-genome genes and C-genome species (*B. oleracea*, *B. napus*). PCA was carried out using logistic singular value decomposition (SVD). In both cases 31% of variance was explained by the model.

varied in abundance between the *B. napus* A and C subgenomes. For example, DNA/Helitron elements constitute 20.4% to 35% of the *B. napus* A subgenome but only 15% to 24.4% of the *B. napus* C subgenome, though they are similarly abundant in the diploid ancestors (22.5% to 27.9% in *B. rapa*, 22.5% to 23.9% in *B. oleracea*). The number of Helitrons observed here is higher than an earlier investigation into Helitrons in Brassicaceae (Hu *et al.*, 2019) due to different computational analysis tools used. It is possible that the Helitrons found here are an overestimate of the true Helitron content as the accurate prediction of Helitrons remains challenging (Ou *et al.*, 2019).

Class II DNA transposons of superfamily CACTA (DNA/DTC) make up between 1.9% to 2.4% of the *B. oleracea* genome and 0.9% to 1.4% of the *B. rapa* genome. We observed an increased number of CACTA transposons in the *B. napus* C subgenome compared to *B. oleracea* (2.4% compared with 1.9%). The greater abundance of CACTA elements in *B. oleracea* compared to *B. rapa* has been observed before (Alix *et al.*, 2008) and CACTA elements have undergone several rounds of amplification since *B. rapa* and *B. oleracea* divergence. Similar CACTA expansions have been observed in amphidiploid cotton compared with its diploid ancestors (Chen *et al.*, 2020b), though in our study the difference may be due to repetitive elements collapsing in the *B. oleracea* assembly, while they were assembled correctly in the more complete *B. napus* assembly. A recent high-quality genome of *B. napus* cv. ZS11 (Chen *et al.*, 2020a) found similar recent repeat expansions compared to the diploid ancestor which supports our findings.

Factors influencing gene loss propensity in the three pangenomes

We examined factors that may influence gene loss propensity. We built models that used genomic features to predict gene loss propensity in the three pangenomes to ask which genomic features have the largest impact on gene loss. These features include distance from centromeres (Mason *et al.*, 2016), gene size, pseudomolecule size, distance from transposons, and in *B. napus*, whether a gene is located in a block syntenic with the homoeologous genome (Figure S8), using genes located only on pseudomolecules and ignoring *B. napus* genes only variable in synthetic lines. This builds on previous observations in *B. oleracea* showing that dispensable *R*-genes are closer to transposable elements than expected (Bayer *et al.*, 2019), frequent nonreciprocal homoeologous exchanges between chromosomes in *B. napus* (Sharpe *et al.*, 1995), and lineage-specific gene loss propensity across eukaryotes (Krylov *et al.*, 2003). We compared five different statistical and machine learning approaches (Logistic Regression, Gaussian Naïve Bayes, Random Forest, AdaBoost and XGBoost) and settled on gradient boosting models (XGBoost) because this model showed the highest accuracy (0.86) and F1-score (0.23) (Table S13). We built gradient boosting models predicting gene loss propensity while accounting for the strong class imbalance by using different sample weights, balancing of positive and negative weights, stratified test and training data, and a Bayesian hyperparameter search to optimize model parameters. These models achieved an accuracy of 85% (AUC: 0.7, average precision-recall score: 0.2, F1: 0.18) in *B. napus*, 88% in *B. oleracea* (AUC: 0.6, average precision-recall score: 0.1, F1: 0.01) and 86% in *B. rapa* (AUC: 0.6, average precision-recall score: 0.14, F1: 0.02) (Figure S9). Confusion matrices revealed that all models had an almost 99% accuracy in predicting whether a gene is core (98% accuracy in *B. napus*), but poor accuracy in predicting whether a gene is dispensable (16% accuracy in *B. napus*) (Table S14). This indicates that the features used in these models do not fully explain gene loss, but explain the extent of gene retention. It is possible that a portion of gene loss in *Brassica* is truly random, in which case the model has no means to explain gene loss. Another possible reason for the low predictability of variable genes in this model is that there are different types of variable genes that we currently cannot distinguish. Genes that are lost due to homeologous recombination are indistinguishable from novel genes created by Helitrons copying exons in the genome.

There may be yet-undiscovered features linked with gene loss that we have not incorporated in the model. Recent studies using synthetic *B. napus* lines suggest that the pattern of homoeologous exchanges is predictable on the chromosome level (Bird *et al.*, 2019) which indicates that incorporating additional, not yet generated data may improve the model's accuracy.

We assessed feature importance for each of the three models using Shapley Additive Explanation (SHAP) (Lundberg and Lee, 2017) values. A large positive SHAP value for a feature indicates that the higher the feature value, the more likely the model is to predict a variable gene. A large negative SHAP value indicates that the higher the feature value, the more likely the model is to predict a core gene. A small SHAP value around 0 indicates no association between the feature and the prediction. The features with the strongest impact on gene loss propensity were the length of the chromosome the gene was located on and the distance from the centromeres. In the diploid pangenomes,

proximity to transposable elements was among 13 and 12 of the top 20 predictors of gene loss propensity in *B. rapa* and *B. oleracea*, respectively; however, in the *B. napus* pangenome-based model, transposable elements appeared only three times within the top 20 strongest predictors. In *B. napus*, membership in homoeologous blocks and position on different chromosomes were among the strongest ten predictors (Figure 4). This suggests that different mechanisms of gene loss dominate in the diploids and the amphidiploids, with homoeologous exchanges being most strongly linked with gene dispensability in *B. napus*, and transposable elements being most strongly linked with gene dispensability in *B. rapa* and *B. oleracea* (Figure 4).

We examined which rare factors have an impact on the prediction of gene loss propensity using the in-built F-score of XGBoost. In *B. rapa*, the strongest rare predictors of gene loss propensity were the presence of LTR and Helitron repeats, while in *B. oleracea* MITEs, LTRs and Helitron repeats were predominant (Figure S10). In *B. napus*, MITEs and pseudomolecule position were the strongest predictors of gene loss propensity. Interestingly, MITEs were common factors between *B. oleracea* and *B. napus*, suggesting that they play a greater role in the shared C genome.

When plotting the importance of 'distance to centromere' for each pseudomolecule separately, the *B. napus* model shows a clear pattern of increasing loss propensity distal to the centromeres, while in the corresponding plots for *B. oleracea* and *B. rapa*, gene loss propensity is distributed across the pseudomolecules (Figure 5). In wheat and *B. napus*, HEs show a similar pattern, with a greater number of HEs towards the telomeres (Zhang *et al.*, 2020), and again indicates the importance of homoeologous recombination in predicting dispensable gene status in *B. napus*.

Subgenome dominance is a well-established phenomenon in polyploids and has previously been observed for specific regions in *B. napus* (Wu *et al.*, 2018; Xie *et al.*, 2019; Zhou *et al.*, 2016). However, studies of subgenome dominance differ in their methodology, with some focusing on differences in gene expression between homoeologous gene-pairs, and others on gene loss. It has been shown that A subgenome regions are more likely to be replaced by C subgenome regions following homoeologous recombination (Bird *et al.*, 2019; Hurgobin *et al.*, 2018) but it is currently unclear if this is related to subgenome expression dominance.

Within *B. napus*, subgenome dominance has usually been observed through differences in gene expression levels between subgenomes (Bird *et al.*, 2019) though it has also been associated with differential gene loss between the subgenomes (Hurgobin *et al.*, 2018). Differential gene loss has also been linked to subgenome dominance in the tetraploid ancestors of *A. thaliana* (Thomas *et al.*, 2006) and maize (Woodhouse *et al.*, 2010). The pseudomolecules C01, C02 and C09 have the strongest association with gene loss propensity among the pseudomolecules tested. This agrees with previous observations showing preferential homoeologous exchange from the A subgenome to the C subgenome in *B. napus* (Hurgobin *et al.*, 2018). Interestingly, these three chromosomes are also the fourth, second and third-longest chromosomes in *B. napus*, suggesting that preferential loss may be associated with longer chromosomes, as previously observed (Chalhoub *et al.*, 2014). However, the longest chromosome, C03, does not appear in the ranking of chromosomes associated with gene loss, suggesting that other mechanisms such as selection may prevent genes on C03 from being lost.

Additional information such as variation in chromosome architecture and behaviour (e. g. crossover frequency) is likely to improve the accuracy of our models, as seen in *B. rapa/B. oleracea* where gene retention is associated with three-dimensional chromosomal organization (Xie *et al.*, 2019).

This study provides insights into the evolution of *Brassica* genomes through a comparative analysis of gene presence/absence variation at the species level. We have shown that gene loss propensity differs between the diploid progenitors of *B. napus* and highlight the genomic differences between synthetic and natural *B. napus* lines. We built models linking the physical location of genes with their gene loss propensity. These models show that the position of a gene on the chromosome is the strongest predictor of gene loss propensity in polyploid *B. napus*, while transposable elements have a greater role in gene loss in the diploids. These results pave the way for the application of machine learning methods to understanding the underlying biological and physical causes of gene presence/absence.

Methods

A new Darmor-*Bzh* reference genome

A new *Brassica napus* cv. Darmor-*bzh* reference genome assembly was assembled by NRGene using the DeNovoMAGICTM software platform (NRGene, Nes Ziona, Israel), a proprietary *DeBruijn* graph-based assembler. This assembler used paired-end Illumina reads (450 and 800 bp insert sizes) along with mate-paired Illumina reads (2–4 and 8–10 kb insert sizes) with a total coverage >180×. Scaffolds were joined using 80× of 10× Chromium data and manually corrected using published genetic maps (Chalhoub *et al.*, 2014). The scaffolds were ordered into pseudomolecules using the v4 assembly (Chalhoub *et al.*, 2014) and RaGOO v1.02 (Alonge *et al.*, 2019). Gene space completeness of both assemblies was assessed using BUSCO v5.1.2 (database: viridiplantae_odb10) (Simão *et al.*, 2015). The two assemblies were aligned using minimap2 v2.18 and differences were visualized using pafv0.0.2 (<https://github.com/dwinter/pafv0.0.2>). Repeats in the new Darmor-*bzh* assembly and the v4 assembly were searched using EDTA v1.9.6 (Ou *et al.*, 2019) and mapped using RepeatMasker v2.0 (Smit and Hubley, 2008).

Construction of three new pangenomes

We assembled three pangenomes for *B. napus*, *B. oleracea* and *B. rapa* using the approach of Golicz *et al.*, (2016). We used publicly available paired-end Illumina reads with more than 9× coverage (except the reference cultivar Darmor-*bzh*) of 87, 77 and 59 individuals for *B. oleracea*, *B. rapa* and *B. napus* respectively (Tables S15). We sequenced 20 additional *B. napus* individuals using Illumina HiSeq 3000 (PRJNA613532). This number of individuals is sufficient to capture the majority of gene content in the population as in previous pangenome assemblies, the rate with which novel gene content increases with each added individuals stops growing after 10 to 50 individuals (Gao *et al.*, 2019; Golicz *et al.*, 2016; Hurgobin *et al.*, 2018; Montenegro *et al.*, 2017).

We aligned these three datasets separately to the new *B. napus* assembly, the v2.1 *B. oleracea* assembly (Parkin *et al.*, 2014) and the v3.0 *B. rapa* assembly (Zhang *et al.*, 2018) respectively. Bowtie2 v2.2.9 (Langmead and Salzberg, 2012) was used for all read alignments (options: `-end-to-end, -sensitive`). The three sets of reads that did not align were assembled using MaSuRCA v3.2.3 (Zimin *et al.*, 2013) into three pangenomes: one

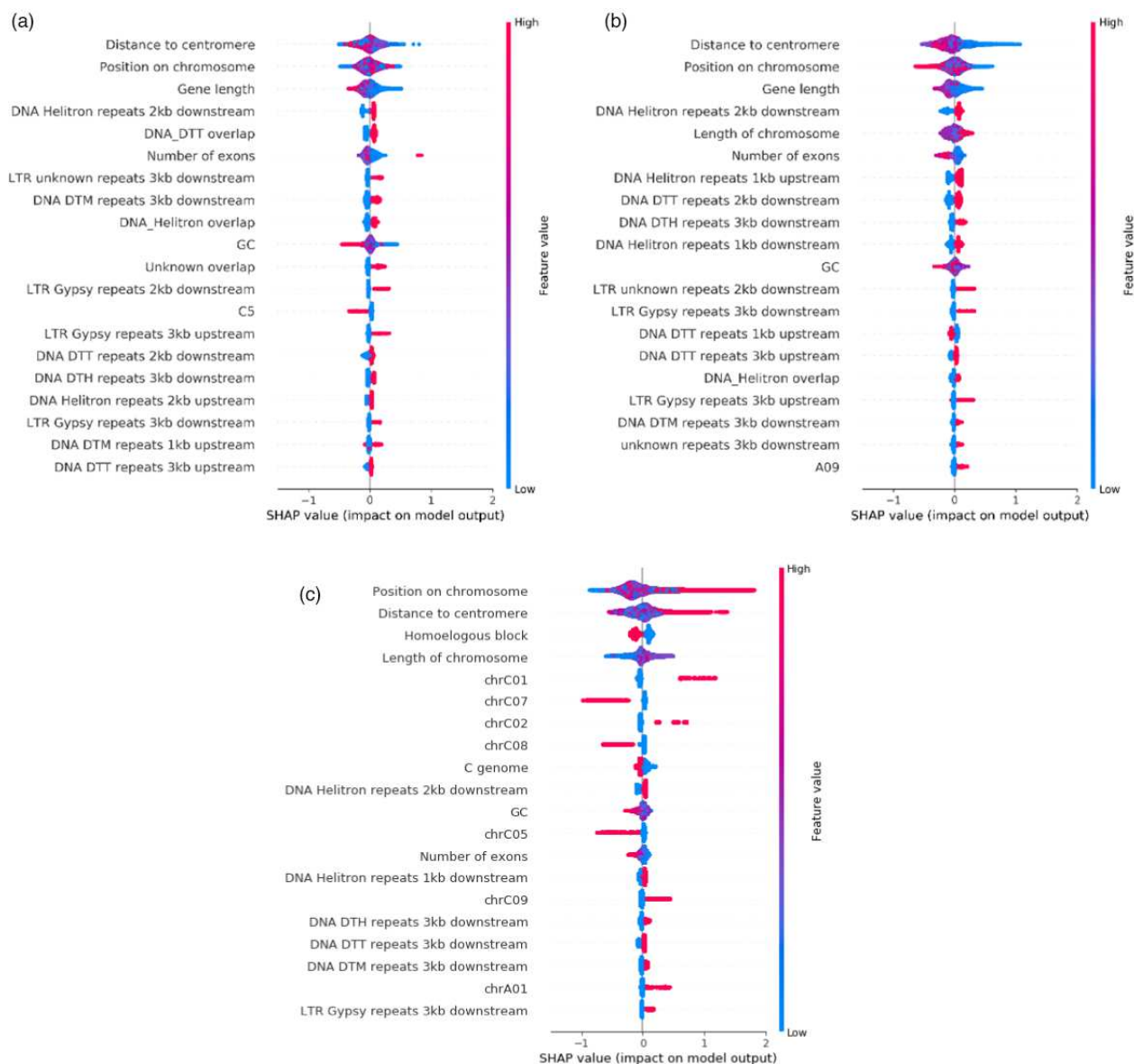


Figure 4 Impact of model output for the prediction of gene loss propensity measured via SHAP values for three XGBoost models trained for PAV data from *B. oleracea* (a), *B. rapa* (b) and *B. napus* (c). High feature values are displayed in red, low in blue. Twenty attributes with the strongest impact on the model are displayed. Binary variables are 1/0 encoded, so genes with a 1 for the dispensable C01 are located on the chromosome C01. In this case, high (red colour) with high SHAP values means that the presence of a gene on this chromosome is a stronger predictor of gene dispensability. The transposable element codes follow the nomenclature of (Wicker *et al.*, 2007): DNA/DTT = CACTA, DNA/DTM = Mutator, DNA/DTH = PIF-Harbinger.

for *B. oleracea* using only *B. oleracea* individuals, one for *B. rapa* using only *B. rapa* individuals, and one for *B. napus* using only *B. napus* individuals. The resulting contigs were aligned with NCBI-NR (accessed 2nd June 2019) using blast+ v2.5.0 (Camacho *et al.*, 2009), and contigs with best hits outside the Viridiplantae were considered to be contamination and removed from subsequent steps.

Gene prediction

For each species pangenome and the reference genome, all publicly available paired RNASeq data (Table S16) were used in the BRAKER v2.0 (Hoff *et al.*, 2019) gene prediction pipeline after each pangenome was soft-masked using RepeatModeler (Smit

and Hubley, 2008) and RepeatMasker (Smit *et al.*, 1996) to avoid removing true genes (Bayer *et al.*, 2018). BRAKER produces AUGUSTUS (Stanke *et al.*, 2006) and GeneMark-EX (Lomsadze *et al.*, 2014) gene predictions. All RNASeq data were aligned using HISAT2 v2.1.0 (Kim *et al.*, 2019) and converted into genome coordinates using StringTie v1.3.4 (Pertea *et al.*, 2015). The RNASeq alignment coordinates were used together with RepeatModeler-based repeat regions, AUGUSTUS and GeneMark-EX predictions, and gene models of the already published *B. oleracea* v2.1 (Parkin *et al.*, 2014), *B. rapa* v3 (Zhang *et al.*, 2018) and *B. napus* v4 (Chalhoub *et al.*, 2014) in the EVidenceModeler v1.1.1 (Haas *et al.*, 2008) pipeline to produce final gene models. Gene models without RNASeq

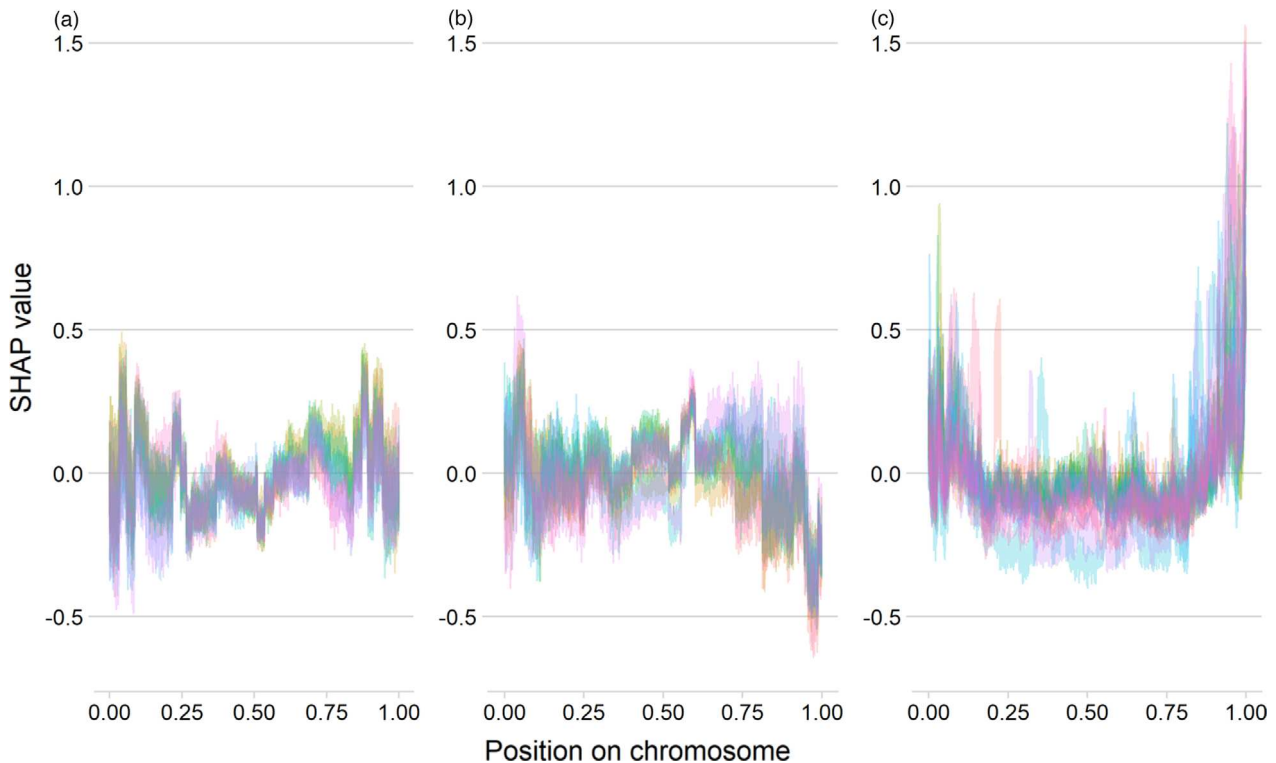


Figure 5 SHAP values as a measure of importance in predicting dispensable genes based on the genes' position on the chromosomes in three XGBoost models trained for *B. oleracea* (a), *B. rapa* (b) and *B. napus* (c). The x-axis represents the feature 'Position on chromosome' in Figure 4. Each line represents one chromosome. The y-axis displays SHAP values, the higher the value, the more of an impact that gene's position has towards the prediction of a dispensable gene. Negative SHAP values imply that this gene's position has an impact towards the prediction of a core gene. Only on *B. napus* do SHAP values exceed 1, and then only at the telomeres of almost all chromosomes. In the diploids, genes located at the telomeres have negative SHAP values, i.e. their telomeres are not linked with the prediction of gene loss propensity.

support and no hits in the previously published gene models were removed from the final annotation. Disease resistance gene analogue (RGA) candidates were predicted using RGAugury (Li *et al.*, 2016).

Gene presence/absence calling

Gene presence/absence variation (PAV) was called using an approach based on SGSGeneLoss (Golicz *et al.*, 2015). For each of the three pangenomes, we aligned all *B. oleracea*, *B. rapa* and *B. napus* reads using Bowtie2 v2.2.9 (Langmead and Salzberg, 2012). Mosdepth v0.2.2 (Pedersen and Quinlan, 2018) and bedtools v 2.27.0 (Quinlan and Hall, 2010) were used to calculate the coverage of all gene exons. Genes where all exon bases were covered by fewer than 2 reads and where the exons' length was covered by less than 5% of their total length were deemed to be absent. While this may lead to some genes being incorrectly classified as present when they are absent, these parameters provide confidence that absent gene calls are truly absent. We used these results to calculate three PAV tables: one for the *B. oleracea* pangenome containing gene presence information all *B. oleracea*, *B. rapa* and *B. napus* individuals, one for the *B. rapa* pangenome containing gene presence information for all *B. oleracea*, *B. rapa* and *B. napus* individuals, and one for the *B. napus* pangenome containing gene presence information for all *B. oleracea*, *B. rapa* and *B. napus* individuals.

PAV-based PCA modelling of dispensable and core genes and GO-enrichment were performed using R v3.6.3 (R Core Team,

2020) using the packages logisticPCA (Landgraf and Lee, 2015), minpack.lm (Elzhov *et al.*, 2010) and topGO (Alexa and Rahnenführer, 2009). GO-terms were assigned to all proteins using PANNZER2 (Törönen *et al.*, 2018) (accessed 5.7.2020, database: Viridiplantae). For each possible number of combinations of genomes, 500 000 pairs were chosen for the modelling of pangenome and core gene numbers.

Proteins were compared using DIAMOND v0.9.29.130 with the STRING v11 *Arabidopsis* database (Szklarczyk *et al.*, 2019) to find proteins within functional networks. Association between network membership and gene status was assessed using the function `chisq.test()` implemented in R v3.6.3 (R Core Team, 2020). Genes were located within syntenic blocks by self-comparison of the *B. napus* annotation using MCScanX (Wang *et al.*, 2012).

Assessing gene loss propensity using machine learning

Gene absence was predicted by building three separate feature tables for the three genomes, using genes located on pseudomolecules only, and genes that are lost in at least 2 individuals. The feature tables contained for each gene: which pseudomolecule the gene is located on, GC content, distance to the end of the pseudomolecule, overlap/1kb/2kb/3kb distance to *de novo* predicted transposon-classes as predicted by EDTA v1.9.6 (Ou *et al.*, 2019), distance to the centromeres as described in (Mason *et al.*, 2016), and, for *B. napus*, whether a gene was located within a syntenic block. Genes variable only in synthetic

individuals were assumed to be core. Accuracy, F1-score and AUC-scores were compared between five machine learning approaches (logistic regression, Gaussian Naïve Bayes, Random Forest, AdaBoost and XGBoost). Three different XGBoost v1.0.2 models (Chen and Guestrin, 2016) were trained using the three PAV feature tables for the *B. oleracea*, *B. rapa* and *B. napus* pangenomes. For this we removed the PAV information of the other species – i.e. the *B. oleracea* pangenome gene feature table contained only information as to whether a gene was variable of *B. oleracea* individuals, not *B. rapa* or *B. napus* individuals.

Scikit-learn v0.21.3 (Pedregosa et al., 2011) was used to calculate supporting statistics such as F1-score, receiver operating characteristic curves and prediction accuracy. The feature table was split into an 80/20 training/test dataset while stratifying for the gene PAV output using scikit-learn's `train_test_split()` function with a random state of 123. Sample weights were computed using the `compute_sample_weight` function in scikit-learn. The following XGBoost parameters were optimized using scikit-optimize BayesSearchCV: `learning_rate` (step size shrinkage used in updates to prevent overfitting), `min_child_weight` (minimum sum of instance weight needed in child, used to decide whether to stop partitioning), `max_depth` (maximum depth of a tree), `max_delta_step` (maximum delta step for each leaf update), `subsample` (subsample ratio of all training instances), `colsample_by_tree` (subsample ratio of columns when constructing trees), `colsample_by_level` (subsample ratio of columns for each level), `reg_lambda` (L2 regularization term on weights), `reg_alpha` (L1 regularization term on weights), `gamma` (minimum loss reduction required to make a further partition), `n_estimators` (number of trees in the model) and `scale_pos_weight` (controls the balance of positive and negative weights) (Head et al., 2018). Model metrics were calculated using the scikit-learn functions `confusion_matrix`, `accuracy_score`, `roc_auc_score` and `f1_score`. Feature importance in the trained models was assessed using TreeExplainer in Shapley Additive Explanations (SHAP) v0.31.0 (Lundberg and Lee, 2017).

Acknowledgements

This work is funded by the Australia Research Council (Projects DP1601004497, LP140100537 and LP130100925), and resources provided by the Pawsey Supercomputing Centre with funding from the Australian Government and the Government of Western Australia. Dr. Philipp Bayer acknowledges the support of the Forrest Research Foundation. YP Lim was supported by Korea Institute of Planning and Evaluation for Technology in Food, Agriculture, and Forestry (IPET) through Golden Seed Project (213006-05-4-SB110), funded by Ministry of Agriculture, Food and Rural Affairs (MAFRA), Ministry of Oceans and Fisheries (MOF), Rural Development Administration (RDA) and Korea Forest Services (KFS), South Korea.

Conflict of Interests

The authors declare no conflict of interests.

Author Contributions

PEB conceived the research. PEB, AS, AAG, YY and RA carried out the research.

SF, HL, HSC, IB, HR, SR, LJ, SL, MSB, ES, XW, GJK, JCP, BC, WJS and contributed to the genome assembly. YPL contributed

additional *B. rapa* seeds. PEB, JB and DE co-wrote the manuscript. All authors read and contributed to the manuscript.

Data availability

All code generated for this study is available at https://github.com/AppliedBioinformatics/Brassica_oleracea_rapa_napus_code

All data generated for this study is available at BioProject PRJNA613532. The assemblies, annotations, PAV-matrices and other supporting data are available at <https://doi.org/10.26182/5f1936836a1c4> and <http://brassicagenome.net/databases.php>. JBrowse (Buels et al., 2016) and KnetMiner (Hassani-Pak et al., 2020) instances are available at <http://brassicagenome.net/databases.php>.

References

- Adams, K.L., Cronn, R., Percifield, R. and Wendel, J.F. (2003) Genes duplicated by polyploidy show unequal contributions to the transcriptome and organ-specific reciprocal silencing. *Proc. Natl Acad. Sci. USA*, **100**, 4649–4654.
- Alexa, A. and Rahnenführer, J. (2009) Gene set enrichment analysis with topGO. *Bioconductor Improve*, **27**, 1–26.
- Alix, K., Joets, J., Ryder, C.D., Moore, J., Barker, G.C., Bailey, J.P., King, G.J. et al. (2008) The CACTA transposon Bot1 played a major role in *Brassica* genome divergence and gene proliferation. *Plant J.* **56**, 1030–1044.
- Allainguillaume, J., Alexander, M., Bullock, J., Saunders, M., Allender, C.J., King, G., Ford, C.S. et al. (2006) Fitness of hybrids between rapeseed (*Brassica napus*) and wild *Brassica rapa* in natural habitats. *Mol. Ecol.* **15**, 1175–1184.
- Allender, C.J. and King, G.J. (2010) Origins of the amphiploid species *Brassica napus* L. investigated by chloroplast and nuclear molecular markers. *BMC Plant Biol.* **10**, 54.
- Alonge, M., Soyk, S., Ramakrishnan, S., Wang, X., Goodwin, S., Sedlazeck, F.J., Lippman, Z.B. et al. (2019) RaGOO: fast and accurate reference-guided scaffolding of draft genomes. *Genome Biol.* **20**, 1–17.
- An, H., Qi, X., Gaynor, M.L., Hao, Y., Gebken, S.C., Mabry, M.E., McAlway, A.C. et al. (2019) Transcriptome and organellar sequencing highlights the complex origin and diversification of allotetraploid *Brassica napus*. *Nat. Commun.* **10**, 2878.
- Bayer, P.E., Edwards, D. and Batley, J. (2018) Bias in resistance gene prediction due to repeat masking. *Nat. Plants*, **4**, 762.
- Bayer, P.E., Golicz, A.A., Tirnaz, S., Chan, C.K., Edwards, D. and Batley, J. (2019) Variation in abundance of predicted resistance genes in the *Brassica oleracea* pangenome. *Plant Biotechnol. J.* **17**, 789–800.
- Bayer, P.E., Golicz, A.A., Scheben, A., Batley, J. and Edwards, D. (2020) Plant pan-genomes as the new reference. *Nat. Plants* **6**, 914–920.
- Berkman, P.J., Visendi, P., Lee, H.C., Stiller, J., Manoli, S., Lorenc, M.T., Lai, K. et al. (2013) Dispersion and domestication shaped the genome of bread wheat. *Plant Biotechnol. J.* **11**, 564–571.
- Bird, K.A., Niederhuth, C., Ou, S., Gehan, M., Chris Pires, J., Xiong, Z., VanBuren, R. et al. (2019) *Replaying the evolutionary tape to investigate subgenome dominance in allopolyploid Brassica napus*. bioRxiv, 814491.
- Brands, A. and Ho, T.H. (2002) Function of a plant stress-induced gene, *HVA22*. Synthetic enhancement screen with its yeast homolog reveals its role in vesicular traffic. *Plant Physiol.* **130**, 1121–1131.
- Buels, R., Yao, E., Diesh, C.M., Hayes, R.D., Munoz-Torres, M., Helt, G., Goodstein, D.M. et al. (2016) JBrowse: a dynamic web platform for genome visualization and analysis. *Genome Biol.* **17**, 66.
- Camacho, C., Coulouris, G., Avagyan, V., Ma, N., Papadopoulos, J., Bealer, K. and Madden, T.L. (2009) BLAST+: architecture and applications. *BMC Bioinformatics*, **10**, 421.
- Chalhoub, B., Denoeud, F., Liu, S., Parkin, I.A., Tang, H., Wang, X., Chiquet, J. et al. (2014) Early allopolyploid evolution in the post-Neolithic *Brassica napus* oilseed genome. *Science*, **345**, 950–953.
- Chen, T. and Guestrin, C. (2016) Xgboost: a scalable tree boosting system. *Proceedings of the 22nd ACM Sigkdd International Conference on Knowledge Discovery and Data Mining*, pp. 785–794. ACM, New York, NY, USA.

- Chen, X., Tong, C., Zhang, X., Song, A., Hu, M., Dong, W., Chen, F. *et al.* (2020a) A high-quality *Brassica napus* genome reveals expansion of transposable elements, subgenome evolution and disease resistance. *Plant Biotechnol. J.* **19**, 615–630.
- Chen, Z.J., Sreedasyam, A., Ando, A., Song, Q., De Santiago, L.M., Hulse-Kemp, A.M., Ding, M. *et al.* (2020b) Genomic diversifications of five *Gossypium* allopolyploid species and their impact on cotton improvement. *Nat. Genet.* **52**, 525–533.
- Cheng, F., Wu, J. and Wang, X. (2014) Genome triplication drove the diversification of *Brassica* plants. *Hortic. Res.* **1**, 14024.
- Edger, P.P., Poorten, T.J., VanBuren, R., Hardigan, M.A., Colle, M., McKain, M.R., Smith, R.D. *et al.* (2019) Origin and evolution of the octoploid strawberry genome. *Nat. Genet.* **51**, 541–547.
- Edger, P.P., Smith, R., McKain, M.R., Cooley, A.M., Vallejo-Marin, M., Yuan, Y., Bewick, A.J. *et al.* (2017) Subgenome dominance in an interspecific hybrid, synthetic allopolyploid, and a 140-year-old naturally established neo-allopolyploid monkeyflower. *Plant Cell*, **29**, 2150–2167.
- Elzhov, T.V., Mullen, K.M. and Bolker, B. (2010) *R interface to the Levenberg-Marquardt nonlinear least-squares algorithm found in MINPACK. Plus Support for Bounds.* 1.2-1.
- Gao, C., Zhou, G., Ma, C., Zhai, W., Zhang, T., Liu, Z., Yang, Y. *et al.* (2016) Helitron-like transposons contributed to the mating system transition from out-crossing to self-fertilizing in polyploid *Brassica napus* L. *Sci. Rep.* **6**, 33785.
- Gao, L., Gonda, I., Sun, H., Ma, Q., Bao, K., Tieman, D.M., Burzynski-Chang, E.A. *et al.* (2019) The tomato pan-genome uncovers new genes and a rare allele regulating fruit flavor. *Nat. Genet.* **51**, 1044–1051.
- Golicz, A.A., Bayer, P.E., Barker, G.C., Edger, P.P., Kim, H., Martinez, P.A., Chan, C.K. *et al.* (2016) The pangenome of an agronomically important crop plant *Brassica oleracea*. *Nat. Commun.* **7**, 13390.
- Golicz, A.A., Martinez, P.A., Zander, M., Patel, D.A., Van De Wouw, A.P., Visendi, P., Fitzgerald, T.L. *et al.* (2015) Gene loss in the fungal canola pathogen *Leptosphaeria maculans*. *Funct. Integr. Genomics*, **15**, 189–196.
- Haas, B.J., Salzberg, S.L., Zhu, W., Pertea, M., Allen, J.E., Orvis, J., White, O. *et al.* (2008) Automated eukaryotic gene structure annotation using EvidenceModeler and the Program to Assemble Spliced Alignments. *Genome Biol.* **9**, R7.
- Hassani-Pak, K., Singh, A., Brandizi, M., Hearnshaw, J., Amberkar, S., Phillips, A.L., Doonan, J.H. and Rawlings, C. (2020) *KnetMiner: a comprehensive approach for supporting evidence-based gene discovery and complex trait analysis across species.* *bioRxiv*.
- Head, T., MechCoder, L. and Shcherbatyi, I. (2018) *scikit-optimize/scikit-optimize: v0.5.2.* *Zenodo*.
- Hoff, K.J., Lomsadze, A., Borodovsky, M. and Stanke, M. (2019) Whole-genome annotation with BRAKER. *Methods Mol. Biol.* **1962**, 65–95.
- Hu, K., Xu, K., Wen, J., Yi, B., Shen, J., Ma, C., Fu, T. *et al.* (2019) Helitron distribution in Brassicaceae and whole genome Helitron density as a character for distinguishing plant species. *BMC Bioinformatics*, **20**, 1–20.
- Hübner, S., Bercovich, N., Todesco, M., Mandel, J.R., Odenheimer, J., Ziegler, E., Lee, J.S. *et al.* (2019) Sunflower pan-genome analysis shows that hybridization altered gene content and disease resistance. *Nat. Plants*, **5**, 54.
- Hurgobin, B. and Edwards, D. (2017) SNP discovery using a pangenome: has the single reference approach become obsolete? *Biology*, **6**, 21.
- Hurgobin, B., Golicz, A.A., Bayer, P.E., Chan, C.K.K., Timaz, S., Dolatabadian, A., Schiessl, S.V. *et al.* (2018) Homoeologous exchange is a major cause of gene presence/absence variation in the amphidiploid *Brassica napus*. *Plant Biotechnol. J.* **16**, 1265–1274.
- Kim, D., Paggi, J.M., Park, C., Bennett, C. and Salzberg, S.L. (2019) Graph-based genome alignment and genotyping with HISAT2 and HISAT-genotype. *Nat. Biotechnol.* **37**, 907–915.
- Kitashiba, H. and Nasrallah, J.B. (2014) Self-incompatibility in Brassicaceae crops: lessons for interspecific incompatibility. *Breed. Sci.* **64**, 23–37.
- Krylov, D.M., Wolf, Y.I., Rogozin, I.B. and Koonin, E.V. (2003) Gene loss, protein sequence divergence, gene dispensability, expression level, and interactivity are correlated in eukaryotic evolution. *Genome Res.* **13**, 2229–2235.
- Landgraf, A.J. and Lee, Y. (2015) *Dimensionality reduction for binary data through the projection of natural parameters.* *arXiv preprint arXiv:1510.06112*.
- Langmead, B. and Salzberg, S.L. (2012) Fast gapped-read alignment with Bowtie 2. *Nat. Methods*, **9**, 357–359.
- Li, P., Quan, X., Jia, G., Xiao, J., Cloutier, S. and You, F.M. (2016) RGAugury: a pipeline for genome-wide prediction of resistance gene analogs (RGAs) in plants. *BMC Genom.* **17**, 852.
- Liu, J., Zhou, R., Wang, W., Wang, H., Qiu, Y., Raman, R., Mei, D. *et al.* (2020a) A copia like-retrotransposon insertion in the upstream region of SHATTERPROOF 1 gene, BnSHP1. A9 is associated with quantitative variation in pod shattering resistance in oilseed rape. *J. Exp. Bot.* **71**, 5402–5413.
- Liu, Y., Du, H., Li, P., Shen, Y., Peng, H., Liu, S., Zhou, G.-A. *et al.* (2020b) Pangenome of wild and cultivated soybeans. *Cell*, **182**, 162–176.e13.
- Lomsadze, A., Burns, P.D. and Borodovsky, M. (2014) Integration of mapped RNA-Seq reads into automatic training of eukaryotic gene finding algorithm. *Nucleic Acids Res.* **42**, e119.
- Lu, K., Wei, L., Li, X., Wang, Y., Wu, J., Liu, M., Zhang, C. *et al.* (2019) Whole-genome resequencing reveals *Brassica napus* origin and genetic loci involved in its improvement. *Nat. Commun.* **10**, 1154.
- Lundberg, S.M. and Lee, S.-I. (2017) A unified approach to interpreting model predictions. *Advances in Neural Information Processing Systems*, pp. 4765–4774. Curran Associates Inc., Red Hook, NY, USA
- Mason, A.S., Rousseau-Gueutin, M., Morice, J., Bayer, P.E., Besharat, N., Cousin, A., Pradhan, A. *et al.* (2016) Centromere locations in *Brassica* A and C genomes revealed through half-tetrad analysis. *Genetics*, **202**, 513–523.
- Montenegro, J.D., Golicz, A.A., Bayer, P.E., Hurgobin, B., Lee, HueyTyng, Chan, C.-K., Visendi, P. *et al.* (2017) The pangenome of hexaploid bread wheat. *Plant J.* **90**, 1007–1013.
- Nagaharu, U. (1935) Genome analysis in *Brassica* with special reference to the experimental formation of *B. napus* and peculiar mode of fertilization. *Jpn J. Botany*, **7**, 389–452.
- Nasrallah, J.B. (1997) Evolution of the *Brassica* self-incompatibility locus: a look into S-locus gene polymorphisms. *Proc. Natl Acad. Sci. USA*, **94**, 9516–9519.
- Ou, S., Su, W., Liao, Y.i., Chougule, K., Agda, J.R.A., Hellings, A.J., Lugo, C.S.B. *et al.* (2019) Benchmarking transposable element annotation methods for creation of a streamlined, comprehensive pipeline. *Genome Biol.* **20**, 1–18.
- Parkin, I.A., Koh, C., Tang, H., Robinson, S.J., Kagale, S., Clarke, W.E., Town, C.D. *et al.* (2014) Transcriptome and methylome profiling reveals relics of genome dominance in the mesopolyploid *Brassica oleracea*. *Genome Biol.* **15**, R77.
- Pedersen, B.S. and Quinlan, A.R. (2018) Mosdepth: quick coverage calculation for genomes and exomes. *Bioinformatics*, **34**, 867–868.
- Pedregosa, F., Varoquaux, G., Gramfort, A., Michel, V., Thirion, B., Grisel, O., Blondel, M. *et al.* (2011) Scikit-learn: Machine learning in Python. *J Machine Learning Res.* **12**, 2825–2830.
- Pele, A., Falque, M., Trotoux, G., Eber, F., Negre, S., Gilet, M., Huteau, V. *et al.* (2017) Amplifying recombination genome-wide and reshaping crossover landscapes in Brassicas. *PLoS Genet.* **13**, e1006794.
- Pertea, M., Pertea, G.M., Antonescu, C.M., Chang, T.C., Mendell, J.T. and Salzberg, S.L. (2015) StringTie enables improved reconstruction of a transcriptome from RNA-seq reads. *Nat. Biotechnol.* **33**, 290–295.
- Quinlan, A.R. and Hall, I.M. (2010) BEDTools: a flexible suite of utilities for comparing genomic features. *Bioinformatics*, **26**, 841–842.
- R Core Team. (2020) *R: A language and environment for statistical computing.* R Foundation for Statistical Computing, Vienna, Austria.
- Rong, J., Feltus, F.A., Liu, L., Lin, L. and Paterson, A.H. (2010) Gene copy number evolution during tetraploid cotton radiation. *Heredity (Edinb)*, **105**, 463–472.
- Schmutz, T., Samans, B., Dyrszka, E., Ulpinnis, C., Weise, S., Stengel, D., Colmsee, C. *et al.* (2015) Species-wide genome sequence and nucleotide polymorphisms from the model allopolyploid plant *Brassica napus*. *Scientific Data*, **2**, 150072.
- Schnable, J.C., Springer, N.M. and Freeling, M. (2011) Differentiation of the maize subgenomes by genome dominance and both ancient and ongoing gene loss. *Proc. Natl Acad. Sci. USA*, **108**, 4069–4074.
- Schoenrock, A., Burnside, D., Moteshareie, H., Pitre, S., Hooshyar, M., Green, J.R., Golshani, A. *et al.* (2017) Evolution of protein-protein interaction networks in yeast. *PLoS One*, **12**, e0171920.
- Sharpe, A., Parkin, I., Keith, D. and Lydiate, D. (1995) Frequent nonreciprocal translocations in the amphidiploid genome of oilseed rape (*Brassica napus*). *Genome*, **38**, 1112–1121.

- Simão, F.A., Waterhouse, R.M., Ioannidis, P., Kriventseva, E.V. and Zdobnov, E.M. (2015) BUSCO: assessing genome assembly and annotation completeness with single-copy orthologs. *Bioinformatics*, **31**, 3210–3212.
- Smit, A.F., Hubley, R. and Green, P. (1996) *2010 RepeatMasker Open-3.0*. <http://www.repeatmasker.org>
- Smit, A.F. and Hubley, R. (2008) *RepeatModeler Open-1.0*. Available from <http://www.repeatmasker.org/>
- Song, J.-M., Guan, Z., Hu, J., Guo, C., Yang, Z., Wang, S., Liu, D. et al. (2020) Eight high-quality genomes reveal pan-genome architecture and ecotype differentiation of *Brassica napus*. *Nat. Plants*, **6**, 34–45.
- Song, K. and Osborn, T.C. (1992) Polyphyletic origins of *Brassica napus*: new evidence based on organelle and nuclear RFLP analyses. *Genome*, **35**, 992–1001.
- Stanke, M., Keller, O., Gunduz, I., Hayes, A., Waack, S. and Morgenstern, B. (2006) AUGUSTUS: ab initio prediction of alternative transcripts. *Nucleic Acids Res.* **34**, W435–439.
- Sun, D., Wang, C., Zhang, X., Zhang, W., Jiang, H., Yao, X., Liu, L. et al. (2019) Draft genome sequence of cauliflower (*Brassica oleracea* L. var. botrytis) provides new insights into the C genome in *Brassica* species. *Hortic. Res.* **6**, 1–11.
- Sun, X.-L., Yu, Q.-Y., Tang, L.-L., Ji, W., Bai, X., Cai, H., Liu, X.-F. et al. (2013) GsSRK, a G-type lectin S-receptor-like serine/threonine protein kinase, is a positive regulator of plant tolerance to salt stress. *J. Plant Physiol.* **170**, 505–515.
- Szklarczyk, D., Gable, A.L., Lyon, D., Junge, A., Wyder, S., Huerta-Cepas, J., Simonovic, M. et al. (2019) STRING v11: protein-protein association networks with increased coverage, supporting functional discovery in genome-wide experimental datasets. *Nucleic Acids Res.* **47**, D607–D613.
- Thomas, B.C., Pedersen, B. and Freeling, M. (2006) Following tetraploidy in an *Arabidopsis* ancestor, genes were removed preferentially from one homeolog leaving clusters enriched in dose-sensitive genes. *Genome Res.* **16**, 934–946.
- Törönen, P., Medlar, A. and Holm, L. (2018) PANNZER2: a rapid functional annotation web server. *Nucleic Acids Res.* **46**, W84–W88.
- Wang, Y., Tang, H., Debarry, J.D., Tan, X., Li, J., Wang, X., Lee, T.H. et al. (2012) MScanX: a toolkit for detection and evolutionary analysis of gene synteny and collinearity. *Nucleic Acids Res.* **40**, e49.
- Wicker, T., Sabot, F., Hua-Van, A., Bennetzen, J.L., Capy, P., Chalhoub, B., Flavell, A. et al. (2007) A unified classification system for eukaryotic transposable elements. *Nat. Rev. Genet.* **8**, 973–982.
- Woodhouse, M.R., Schnable, J.C., Pedersen, B.S., Lyons, E., Lisch, D., Subramaniam, S. and Freeling, M. (2010) Following tetraploidy in maize, a short deletion mechanism removed genes preferentially from one of the two homologs. *PLoS Biol.* **8**, e1000409.
- Wu, D., Liang, Z., Yan, T., Xu, Y., Xuan, L., Tang, J., Zhou, G. et al. (2019) Whole-genome resequencing of a worldwide collection of rapeseed accessions reveals the genetic basis of ecotype divergence. *Mol. Plant*, **12**, 30–43.
- Wu, J., Lin, L., Xu, M., Chen, P., Liu, D., Sun, Q., Ran, L. et al. (2018) Homoeolog expression bias and expression level dominance in resynthesized allopolyploid *Brassica napus*. *BMC Genom.* **19**, 586.
- Xie, T., Zhang, F.-G., Zhang, H.-Y., Wang, X.-T., Hu, J.-H. and Wu, X.-M. (2019) Biased gene retention during diploidization in *Brassica* linked to three-dimensional genome organization. *Nat. Plants*, **5**, 822–832.
- Yang, Z., Gong, Q., Qin, W., Yang, Z., Cheng, Y., Lu, L., Ge, X. et al. (2017) Genome-wide analysis of *WOX* genes in upland cotton and their expression pattern under different stresses. *BMC Plant Biol.* **17**, 113.
- Yu, J., Golicz, A.A., Lu, K., Dossa, K., Zhang, Y., Chen, J., Wang, L. et al. (2019) Insight into the evolution and functional characteristics of the pan-genome assembly from sesame landraces and modern cultivars. *Plant Biotechnol. J.* **17**, 881–892.
- Zhang, L., Cai, X., Wu, J., Liu, M., Grob, S., Cheng, F., Liang, J. et al. (2018) Improved *Brassica rapa* reference genome by single-molecule sequencing and chromosome conformation capture technologies. *Hortic. Res.* **5**, 50.
- Zhang, X., Wang, L., Yuan, Y., Tian, D. and Yang, S. (2011) Rapid copy number expansion and recent recruitment of domains in S-receptor kinase-like genes contribute to the origin of self-incompatibility. *FEBS J.* **278**, 4323–4337.
- Zhang, Z., Gou, X., Xun, H., Bian, Y., Ma, X., Li, J., Li, N. et al. (2020) Homoeologous exchanges occur through intragenic recombination generating novel transcripts and proteins in wheat and other polyploids. *Proc. Natl Acad. Sci. USA*, **117**, 14561–14571.
- Zhao, J., Bayer, P., Ruperao, P., Saxena, R., Khan, A., Golicz, A., Nguyen, H. et al. (2020) Trait associations in the pangenome of pigeon pea (*Cajanus cajan*). *Plant Biotechnol. J.* **18**, 1946–1954.
- Zhao, Q., Feng, Q., Lu, H., Li, Y., Wang, A., Tian, Q., Zhan, Q. et al. (2018) Pan-genome analysis highlights the extent of genomic variation in cultivated and wild rice. *Nat. Genet.* **50**, 278–284.
- Zhou, J., Tan, C., Cui, C., Ge, X. and Li, Z. (2016) Distinct subgenome stabilities in synthesized *Brassica* allohexaploids. *Theor. Appl. Genet.* **129**, 1257–1271.
- Zimin, A.V., Marcais, G., Puiu, D., Roberts, M., Salzberg, S.L. and Yorke, J.A. (2013) The MaSuRCA genome assembler. *Bioinformatics*, **29**, 2669–2677.

Supporting information

Additional supporting information may be found online in the Supporting Information section at the end of the article.

Figure S1 Comparison between the v4.1 assembly (Chalhoub et al., 2014) and the new v9 assembly.

Figure S2 Comparison of repeat content by class in Mbp between the two assemblies showing that the six most abundant classes have roughly doubled in size in the v9 assembly.

Figure S3 Number of core and dispensable genes for the A and the C genome, compared between *B. napus* (with and without synthetic lines) and *B. rapa/B. oleracea*.

Figure S4 (a) NLR-genes compared between *B. napus*, *B. rapa* and *B. oleracea*, along with additional pangenome contigs.

Figure S5 PCA plots based on PAV patterns of genes located on each chromosome in *B. napus* split into subgenomes A and C (subfigures A and B respectively) showing strong divergence in PAV patterns between some chromosomes of the *B. napus* A and the C subgenome, especially C03, C09, A05 and A07.

Figure S6 PCA plot showing divergence of individuals based on gene presence/absence patterns on the A genome. A) chromosome A01, B) A02, C) A03, D) A04, E) A05, F) A06, G) A07, H) A08, I) A09 and J) A10. FPSC: Fast Plants, self-compatible.

Figure S7 PCA plot showing divergence of individuals based on gene presence/absence patterns on the C genome.

Figure S8 Different kinds of reciprocal and non-reciprocal inheritances after homoeologous recombination in *B. napus*.

Figure S9 Receiver-operating curves comparing the three XGBoost models trained on *B. oleracea*, *B. rapa* and *B. napus* data respectively.

Figure S10 Twenty features with the strongest impact on the *B. rapa* (A), *B. oleracea* (B) and *B. napus* (C) models measured by relative quantity as assessed using XGBoost's inbuilt feature importance methods ('cover'), showing that in rare feature attributes, the *B. oleracea* and the *B. rapa* model focus mostly on retrotransposons in its best-predicting attributes, and in *B. napus*, the best predictors are pseudomolecule membership.

Table S1 BUSCO results for *B. napus* v4.1 (Chalhoub et al., 2014) and the new NRGene v9 assembly.

Table S2 Comparison of repeats between *B. napus* v4.1 and v9 assembly.

Table S3 Comparison of repeats between *B. napus* v4.1 and v9 assembly.

Table S4 Comparison of repeats between *B. napus* v4.1 and v9 assembly.

Table S5 Top 15 enriched GO terms in the dispensable genes of *B. oleracea*, *B. rapa*, *B. napus*, and *B. napus* without synthetic lines.

Table S6 Numbers of core and dispensable genes in STRING functional networks without synthetic lines.

Table S7 Count of transposable elements per pseudomolecule in the *B. oleracea* assembly.

Table S8 Total length (Mbp) of transposable elements per pseudomolecule in the *B. oleracea* assembly.

Table S9 Total length (Mbp) of transposable elements as percentage of total pseudomolecule length in the *B. oleracea* assembly.

Table S10 Count of transposable elements per pseudomolecule in the *B. rapa* assembly.

Table S11 Total length (Mbp) of transposable elements per pseudomolecule in the *B. rapa* assembly.

Table S12 Total length (bp) of transposable elements as percentage of total pseudomolecule length in the *B. rapa* assembly.

Table S13 Comparison of models using the *B. napus* gene loss data.

Table S14 Confusion matrix for the three XGBoost models trained on *B. oleracea*, *B. rapa*, and *B. napus* data.

Table S15 Data used for the assembly of the three pangenomes.

Table S16 RNASeq data used for the annotation of the three pangenomes.